PCCP

PAPER

Kinetic study of the reaction of vanadium and vanadium–titanium oxide cluster anions with SO_2

Ewald Janssens,*[a] Sandra M. Lang,†[a] Mathias Brümmer,[b] Andrzej Niedziela,[c]
Gabriele Santambrogio,‡[b] Knut R. Asmis[d] and Joachim Sauer*[c]

The reactivity of mass-selected $V_4O_{10}^-$ cluster anions towards sulphur dioxide is investigated in an ion trap under multi-collision conditions. Gas phase reaction kinetics are studied as a function of temperature (T_R = 150–275 K). The binding energy of SO_2 to $V_4O_{10}^-$ is obtained by analyzing the experimental low pressure rate constants, employing the Lindemann energy transfer model for association reactions in conjunction with statistical RRKM theory. In addition, infrared multiple photon dissociation spectroscopy is used in conjunction with density functional theory for the structural assignment of the [$V_4O_{10}^-$, SO_2] complex, revealing a square pyramidal structure with the SO_2 molecule incorporated in the vanadium oxide framework. Energy profiles are calculated for the reaction between $V_4O_{10}^-$ and $V_6O_{15}^-$ with SO_2. Whereas the transition structures along the reaction pathway of $V_4O_{10}^-$ with SO_2 have energies below those of the separated partners, the reaction of $V_6O_{15}^-$ with SO_2 proceeds *via* a transition structure with energy higher than the educts. The role of cluster size and composition is investigated by studying the reaction kinetics of larger ($V_6O_{15}^-$ and $V_8O_{20}^-$) and titanium doped ($V_3TiO_{10}^-$ and $V_2Ti_2O_{10}^-$) vanadium oxide clusters with SO_2. The observed cluster size and composition dependencies are discussed.

A Introduction

Vanadium oxide has gained much attention as a catalyst over the past years.[1] As an oxidative catalyst V_2O_5 has been used in various processes such as the oxidative dehydrogenation of propane, the formation of maleic anhydride from butane, the selective reduction of NO_x with ammonia, and the regeneration of petroleum refinery cracking catalysts.[2] Also sulphur dioxide is oxidized to sulphur trioxide in the presence of supported vanadium oxide particles. The formation of SO_3 is a key step in the production of sulfuric acid, the most abundant industrially produced compound.[3] For this purpose traditional platinum based catalysts are replaced by low cost V_2O_5 based systems.

The vanadium oxide catalyzed production of SO_3 from SO_2 in industrial reactors is optimal at elevated temperatures

(> 700 K) and involves several steps: the adsorption of SO_2, the oxidation of SO_2 followed by the release of SO_3, and the reoxidation of the vanadium oxide particles.[4]

Despite the important industrial relevance of vanadium oxide particles, many microscopic details of their catalytic behaviour are still unknown. The identification of the active sites with surface characterization techniques is experimentally very challenging. In this respect experiments on gas phase clusters provide an appropriate environment to investigate the influence of composition, cluster size, charge and oxidation state on the reactivity.[5]

Gas phase ion–molecule reactivity studies on mass-selected vanadium oxide clusters have, among others, been performed by the Castleman group[6,7] and by the Schwarz group[8,9] and mainly focused on the interaction of vanadium oxide cluster ions with small hydrocarbons. It was found that the reaction pathways and reaction rates strongly depend on the cluster size and charge state, as well as on the oxidation states of the vanadium atoms. Li *et al.* probed the photo-induced oxygen transfer for ethane adsorbed on $V_4O_{11}^-$ under controlled conditions in an ion trap reactor.[10] Zhao *et al.* studied hydrogen abstraction from *n*-butane on binary vanadium–silicon oxide cluster anions.[11] Two combined experimental and theoretical studies characterized the structures of selected complexes composed of a vanadium oxide cluster and a hydrocarbon reactant. Fielicke *et al.* measured the infrared photodissociation

[a] *Laboratorium voor Vaste-Stoffysica en Magnetisme, KU Leuven, Celestijnenlaan 200D, B-3001 Leuven, Belgium. E-mail: ewald.janssens@fys.kuleuven.be*
[b] *Institut für Experimentalphysik, Freie Universität Berlin, Arnimallee 14, D-14195 Berlin, Germany*
[c] *Institut für Chemie, Humboldt-Universität Berlin, Unter den Linden 6, D-10099 Berlin, Germany. E-mail: js@chemie.hu-berlin.de*
[d] *Fritz-Haber-Institut der Max-Planck-Gesellschaft, Faradayweg 4-6, D-14195 Berlin, Germany*
† Present address: Institut für Oberflächenchemie und Katalyse, Universität Ulm, Albert-Einstein-Allee 47, D-89069 Ulm, Germany.
‡ Present address: Fritz-Haber-Institut der Max-Planck-Gesellschaft, Faradayweg 4-6, D-14195 Berlin, Germany.

14344 | *Phys. Chem. Chem. Phys.*, 2012, **14**, 14344–14353

This journal is © the Owner Societies 2012

spectra of the association complex of $V_2O_{5,6}^+$ with ethylene formed in the expansion of a laser vaporisation source.[12] Wende *et al.* obtained structural information on the reaction products of $V_4O_{10}^+$ with propane in a buffer gas filled ion trap.[13]

Some spectrometric work has been done on the reaction of vanadium oxide clusters with SO_2. Wyrwas studied the interaction of small anionic vanadium oxide clusters in a fast flow reactor as a function of the SO_2 concentration.[14] Incompletely oxidized vanadium clusters were proven to be more reactive than clusters with all vanadium atoms in the formal +v oxidation state. However, no quantitative conclusion could be drawn since also molecular oxygen was present in the flow reactor. Bernstein *et al.* studied the reactions of small neutral vanadium oxide clusters with SO_2 in a fast-flow reactor by time-of-flight mass spectrometry and ultraviolet postionization in combination with density functional theory (DFT) calculations.[15,16] They found indications for the formation of SO_3 on oxygen-rich clusters. Other groups investigated the scattering behaviour of vanadium oxide cluster cations by SO_2, but no special size dependencies were observed.[17]

To fully understand the correlation between cluster structure and reactivity, prior knowledge of the structure of the cluster is indispensable. This information has been gathered on cationic and anionic vanadium oxide clusters by combined vibrational spectroscopy experiments and DFT investigations.[19–24] In particular, it was shown that the anionic $(V_2O_5)_n^-$ (n = 2–4) clusters have high symmetric polyhedral caged structures with vanadyl (V=O) units at the apexes and oxygen atoms bridging the vanadium atoms (V–O–V).[18] In addition, it was demonstrated that the vanadium atoms in $V_4O_{10}^-$ can be substituted by titanium atoms without significant distortion of the tetrahedral caged geometry.[25] Also, the electronic structure of small vanadium oxide clusters was studied with anion photoelectron spectroscopy.[26]

Here we investigate the reaction kinetics of thermalized vanadium oxide and vanadium–titanium oxide cluster anions under multi-collision conditions as a function of the cluster temperature and SO_2 partial pressure. In Section B the experimental method, the data analysis, and the theoretical method are presented. In Section C the interaction of $V_4O_{10}^-$ with SO_2 is discussed in detail by investigating the structure of the $[V_4O_{10}, SO_2]^-$ complex and the associated reaction kinetics. In Section D the possible presence of high-energy transition structures in the reaction energy profile is discussed. Also the cluster size and cluster composition dependency are studied by comparing the reaction kinetics of $V_4O_{10}^-$ with that of $V_6O_{15}^-$, $V_8O_{20}^-$, $V_3TiO_{10}^-$, and $V_2Ti_2O_{10}^-$.

B Methods

B.1 Experimental setup

The experiments to obtain temperature and pressure dependent rate constants were carried out in a tandem mass spectrometer-ion trap system, described in detail elsewhere.[27]

$V_mTi_nO_o^-$ clusters are produced by pulsed laser vaporization of the respective metal targets in the presence of 1% O_2 in

He using a 10 Hz dual laser vaporization source.[28] The beam of negative ions is collimated and mass selection is achieved *via* a first quadrupole mass filter. Mass selected ions are accumulated in a linear radio-frequency ion trap. The trap is continuously filled with a small fraction of the reactant SO_2 (0.002–0.1%) in He at a total pressure of 4–9 Pa using a mass flow controller. Temperature control inside the trap between 20 K and 300 K is achieved with a helium cryostat attached to the trap enclosure. The absolute pressure in the trap is measured with a capacitance manometer (MKS, Baratron) having an accuracy of 0.01 Pa. Since the SO_2 vapour pressure at the lowest investigated temperature of 150 K is about 1 Pa and thus much higher than the partial SO_2 pressure used in the experiments, a significant error on the SO_2 concentration due to freezing can be excluded. The uncertainty in the composition of the diluted gas mixture, however, yields a typical uncertainty in the SO_2 partial pressure of 20–30%, which is the main factor for the uncertainty in the rate constants.

The applied pressures ensure multi-collision conditions in the low pressure regime of chemical kinetics and provide thermalisation, of both reactants and reaction products, within a few milliseconds.[29] This thermalisation time is one to three orders of magnitude smaller than typical ion storage times inside the ion trap. After a defined storage time (reaction time t_R) all ionic reactants, intermediates, and products are extracted from the trap and mass analyzed by a second quadrupole mass filter. Recording the different ion yields as a function of t_R gives time resolved kinetic measurements at a given cluster temperature and SO_2 partial pressure.

The infrared multiple photon dissociation (IRMPD) spectrum of the $[V_4O_{10}, SO_2]^-$ complex is obtained on the same instrument by photoexcitation of the trapped ions with pulsed infrared radiation from the Free Electron Laser for Infrared eXpertiments (FELIX) located at the FOM Institute Rijnhuizen in the Netherlands.[30] The method applied to measure IRMPD spectra has been described elsewhere.[22] The ion trap is filled with mass selected $V_4O_{10}^-$ ions, which are thermalised at 125 K by inelastic collisions with the He buffer gas and reacted with the SO_2 molecules present. FELIX is operated at 5 Hz and applied collinear to the ion trap main axis. Directly after FELIX fires all ions are extracted from the trap and detected mass-selectively. The IRMPD spectrum is recorded by monitoring the fragment ion intensity ($V_4O_{10}^-$). Photoabsorption manifests itself either as maxima in the fragment intensity or as dips in the $[V_4O_{10}, SO_2]^-$ complex ion signal. Spectra measured by recording the $V_4O_{10}^-$ fragment intensity indeed show the same spectral features as the $[V_4O_{10}, SO_2]^-$ complex ion signal. The IR spectrum is recorded in the 570–1100 cm^{-1} (17.5–9.0 μm) range with a 0.02 μm step size.
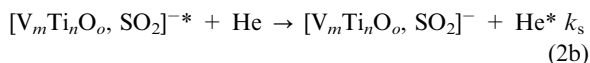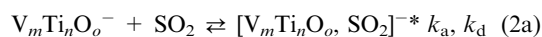
B.2 Analysis of the kinetic traces

The data evaluation procedure to analyze the temperature dependent kinetic traces and the corresponding error analysis is described in detail elsewhere[29,31] and is only briefly summarized here. The normalized kinetic traces are evaluated by fitting the integrated rate equations of proposed reaction mechanisms to the experimental data using the '*Detmech*' software.[32] This leads to the determination of the simplest

This journal is © the Owner Societies 2012

Phys. Chem. Chem. Phys., 2012, **14**, 14344–14353 | 14345

reaction mechanism that fits the experimental data best. The SO_2 ($\sim 10^{11}$ cm^{-3}) and He ($\sim 10^{15}$ cm^{-3}) concentrations are several orders of magnitude larger than the cluster ion concentration ($\sim 10^6$ cm^{-3}) and therefore can be considered constant. Moreover, a continuous inflow of the reaction gas is ensured by the mass flow controller. Thus, the resulting rate constants are pseudo-first order.

Furthermore, the experiments are performed at 4–9 Pa of total pressure and thus in the kinetic low pressure regime. Consequently, each simple association reaction

$$V_mTi_nO_o^- + SO_2 \rightarrow [V_mTi_nO_o, SO_2]^-\ k_f \quad (1)$$
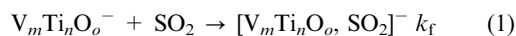
can be described by the Lindemann energy transfer model for association reactions:[33]

$$V_mTi_nO_o^- + SO_2 \rightleftarrows [V_mTi_nO_o, SO_2]^-*\ k_a, k_d \quad (2a)$$

$$[V_mTi_nO_o, SO_2]^-* + He \rightarrow [V_mTi_nO_o, SO_2]^- + He*\ k_s \quad (2b)$$

According to this mechanism, the anionic metal oxide cluster reacts with SO_2, resulting in the formation of an energized intermediate $[V_mTi_nO_o, SO_2]^-*$ with a rate constant k_a. This intermediate may decompose back to the reactants (rate constant k_d) via unimolecular decay or may be stabilized by an energy-transfer collision with He (rate constant k_s). Consequently, the overall forward reaction depends on the He buffer gas and is of third order. In the kinetic low pressure limit, the corresponding measured pseudo-first order rate constant $k_f^{(1)}$ is given by:[31,33]

$$k_f = k_f^{(1)} = k_f^{(3)} [SO_2][He] = (k_a k_s/k_d)[SO_2][He] \quad (3)$$

The ion–molecule association rate constant k_a as well as the stabilization rate constant k_s are well represented by ion–molecule collision rate constants as specified by Langevin theory.[34] k_s only depends on the reduced mass of the $[V_mTi_nO_o, SO_2]^-*$–He 'scattering complex' as well as the polarizability of the He atom ($\alpha = 0.208$ Å^3)[35] and is temperature independent. SO_2 is a polar molecule with a permanent dipole moment $\mu_D = 5.44\ 10^{-30}$ Cm and a polarizability $\alpha = 3.72$ Å^3.[35,36] To estimate k_a, the Langevin rate constant was corrected by a slightly temperature dependent empirical expression found by Su.[37] The resulting temperature dependence of k_a is much smaller than the experimentally observed temperature dependence of k_f, which consequently must be contained in the unimolecular decomposition rate constant k_d.

Applying eqn (2) and (3) allows for the determination of an experimental unimolecular decomposition rate constant k_d which might also be described by RRKM (Rice–Ramsperger–Kassel–Marcus) theory.[38,39] This theory is usually applied to determine k_d from the known binding energy of the ligand to the cluster ion. In our experimental approach k_d is the quantity derived from the experimental data, which consequently allows for the determination of the SO_2 binding energy. In order to obtain RRKM binding energies E_0, k_d was simulated using the 'MassKinetics' software package.[40]

B.3 Theoretical methods

DFT calculations on $[V_4O_{10}, SO_2]^-$ were performed using the TURBOMOLE program.[41] The B3LYP hybrid functional[42] is employed in conjunction with the triple-zeta valence basis sets developed by Ahlrichs and coworkers[43] and augmented by polarization functions: a d-set for oxygen and a p-set for vanadium.[44] Since sulphur requires tight d-functions,[45] the 3d function of the TZVP set for sulphur (0.550) has been replaced by the two d functions (2.994; 0.481) of the cc-pV(D + d)Z basis set.[46]

Initial guesses for transition structures were obtained from scans of appropriate internal coordinates. Starting from those structures the eigenvector following method was applied as implemented in TURBOMOLE. Stationary points found were characterized by harmonic frequency calculations, yielding one imaginary frequency for transition structures. To confirm that an obtained transition structure connects specific minima, this structure was distorted along the imaginary frequency mode in both directions.

Harmonic vibrational frequencies are obtained from second analytic derivatives.[47] To account for both anharmonicities and systematic errors of the calculated harmonic force constants, the computed vibrational frequencies are scaled using scaling factors consistent with our earlier work.[20,22,48] A different scale factor is used for V=O vanadyl modes (0.9167) and V–O–V and other modes (0.9832). The calculated S=O stretching frequencies are scaled by a factor of 1.0206 as derived by comparing the B3LYP/TZVP+d frequencies of SO_2 (1322 and 1139 cm^{-1}) with the experimental values (1362 and 1151 cm^{-1}).[49]

C The reaction of $V_4O_{10}^-$ with SO_2

The reaction of $V_4O_{10}^-$ with SO_2 is chosen as a model system to gain insight into the SO_2 bonding mechanism. First the structure of the $[V_4O_{10}, SO_2]^-$ complex is assigned using IRMPD spectroscopy in conjunction with DFT calculations. Then the reaction energy profile is discussed. It is shown computationally that the adsorption of SO_2 on $V_4O_{10}^-$ is a barrierless process. Thereafter, the temperature dependent reaction kinetics is presented and finally the experimental SO_2 binding energy is derived employing the Lindemann energy transfer mechanism for association reactions in conjunction with RRKM theory.

C.1 Structural assignment of $[V_4O_{10}, SO_2]^-$

The experimental IRMPD spectrum of $[V_4O_{10}, SO_2]^-$, shown in Fig. 1 (bottom trace), exhibits an intensive absorption band at 1003 cm^{-1} with two shoulder peaks on its high energy side at 1029 and 1046 cm^{-1}. In the 700–950 cm^{-1} range there are five distinct absorption bands (at 742, 799, 825, 870, and 900 cm^{-1}).

The IRMPD spectrum of $[V_4O_{10}, SO_2]^-$ strikingly differs from that of the bare $V_4O_{10}^-$ cluster, which is dominated by a single intense vanadyl band at 990 cm^{-1} and has some weaker absorptions around 600–650 cm^{-1}.[18,22] The simplicity of the $V_4O_{10}^-$ IRMPD spectrum is due to its high symmetric tetragonal D_{2d} structure with the unpaired electron being completely delocalized over the d-states of the four vanadium atoms. Localisation of the unpaired electron at a single vanadium site lowers the symmetry and leads to intense V–O–V stretches in the 800–1000 cm^{-1} range.[18] Based on this knowledge the
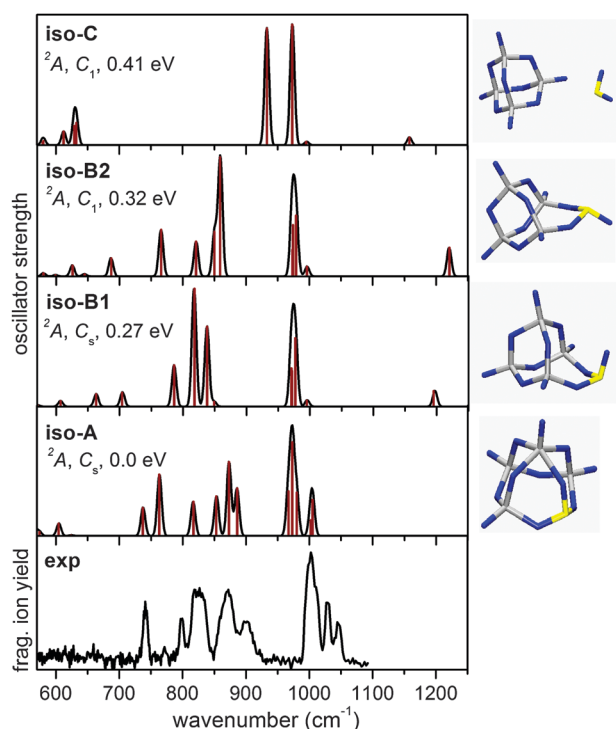
14346 | *Phys. Chem. Chem. Phys.*, 2012, **14**, 14344–14353

This journal is © the Owner Societies 2012

Fig. 1 (Bottom) IRMPD spectrum of $[V_4O_{10}, SO_2]^-$, measured by recording the $V_4O_{10}^-$ fragment intensity in the 570–1100 cm^{-1} range. (Top) Simulated linear IR absorption spectra, based on scaled B3LYP/TZVP+d frequencies and oscillator strengths of four low energy $[V_4O_{10}, SO_2]^-$ isomers. The corresponding structures of the $[V_4O_{10}, SO_2]^-$ isomers are shown on the right (O blue, V grey, and S yellow).

experimental IRMPD spectrum of $[V_4O_{10}, SO_2]^-$ can be interpreted as follows: (i) the absorptions in the 1000–1050 cm^{-1} range correspond to vanadyl modes. The presence of multiple bands in this range suggests that, differently from $V_4O_{10}^-$, the symmetry of the structure is broken. (ii) The absorptions in the 750–950 cm^{-1} range correspond to V–O–V modes (possibly also V–O–S modes) and the unpaired electron is localized in a vanadium d state. This interpretation is confirmed by the results of DFT calculations, which also yield specific structure information.

Simulated linear absorption spectra of four structural isomers predicted by DFT, labeled **A**, **B1**, **B2**, and **C**, are plotted in Fig. 1. The obtained global energetic minimum, **A** (C_s, 0 eV), is a pentameric cluster with a square pyramidal structure resembling the structure of $V_5O_{13}^-$ (C_{4v}).[22] Structures in which SO_2 bridges two OV(O–)$_3$ units, **B1** (C_s, +0.27 eV) and **B2** (C_1, +0.32 eV) can be derived from the bridged C_{2v} structure of $V_5O_{13}^-$ (C_{2v})[22] when replacing the (O=)$_2$V$^{(-)}$(–O)$_2$ unit by (O=)S(–O)$_2$ and putting an unpaired electron in a d-state of one of the vanadium sites. The $V_4O_{10}\cdot SO_2$ encounter complex, **C** (C_1, 0.41 eV), is significantly less stable. Comparison with the IRMPD spectrum indeed shows that the encounter complex is not present in the experiment.

The pyramidal global minimum structure, **A**, is the only isomer without S=O vibrations at wavenumbers above the V=O region. The other isomers have short S=O bonds (146–147 pm) with predicted wavenumbers (1173–1196 cm^{-1})

well above the V=O region (1059–1087 cm^{-1}). The IR spectrum of isomer **A** resembles that of $V_5O_{13}^-$ [ref. 22] and agrees best with the experimental IRMPD spectrum of $[V_4O_{10}, SO_2]^-$. In comparison to $V_5O_{13}^-$, one of the O=VO$_{3/2}$ corners of the square has been replaced by S$^{(+)}$O$_{3/2}$, and the O=V(d^0)$^{(-)}$O$_{4/2}$ top site has been replaced by a O=V(d^1)$^{(2-)}$O$_{4/2}$ site with the unpaired electron localized in the d-states of this vanadium atom, in line with the intuitive interpretation given above. In the 1000–1050 cm^{-1} region, the experimental spectrum seems to have more features (three peaks plus one shoulder) than the simulated spectrum for **A** (two peaks). However, the calculation yields four different vanadyl stretching frequencies, and the DFT calculation may underestimate the energy differences between the four modes. Although the existence of another minimum with similar energy can never be excluded, we feel that for this level of agreement there is no need for applying a global optimization technique such as a genetic algorithm. We note, however, that based on the comparison with the IRMPD spectrum, the presence of (a minor fraction of) isomers **B1** and **B2** in the ion trap cannot be excluded.

C.2 DFT energy profile for the reaction of $V_4O_{10}^-$ with SO_2

The energy profile for the reaction from the educts $V_4O_{10}^-$ and SO_2 to the final product, **A**, has been calculated by DFT. Upon collision of $V_4O_{10}^-$ with SO_2, the encounter complex **C** is formed, which is separated from the "bridging" isomer **B1** by a small barrier, **TS1**. The energy of this transition structure is 0.09 eV below that of the separated $V_4O_{10}^-$ and SO_2. Note that (at least at this computational level) **B1** is not directly reached from **TS1**, but there is an extremely shallow intermediate that has almost the same energy as the second transition structure **TS2**. **B1** further transforms into the square pyramidal ground-state structure, **A**. The SO_2 binding energy in **A** is 0.70 eV.

C.3 Temperature dependent reaction kinetics

Fig. 3(a) displays, as an example, an anion mass distribution obtained after storing $V_4O_{10}^-$ in the presence of SO_2 ($p(SO_2)$ = $(4.4 \pm 1.1) \times 10^{-3}$ Pa) in the ion trap at T_R = 225 K. The kinetic traces in Fig. 3(b)–(d) show the normalized product ion concentrations (open symbols) as a function of reaction time t_R for different reaction temperatures and SO_2 partial pressures. Independent of the reaction temperature (275–150 K), $V_4O_{10}^-$ adsorbs a single SO_2 molecule, forming exclusively $[V_4O_{10}, SO_2]^-$. At the highest investigated temperatures (275 K and 250 K) the reaction is best described by an equilibrium reaction mechanism according to

$$V_4O_{10}^- + SO_2 \rightleftarrows [V_4O_{10}, SO_2]^- \quad k_f, k_b \qquad (4)$$
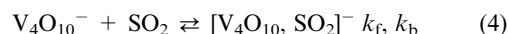
while at lower temperatures the backreaction k_b is hampered and becomes up to two orders of magnitude smaller than k_f. This positive temperature dependence is in line with the Lindemann mechanism[33] that has to be considered to describe the details of the backward reaction step. The solid lines in Fig. 3(b)–(d) are obtained by fitting the integrated rate equations of this proposed reaction mechanism to the experimental kinetic data.

Table 1 Measured termolecular $k_f^{(3)}$ rate constants for the forward reaction between $V_4O_{10}^-$ and SO_2 and corresponding unimolecular decomposition rate constant k_d of the energized complex as function of the reaction temperature T_R

T_R/K	$k_f^{(3)a}$/10^{-28} cm^6 s^{-1}	k_d^a/10^9 s^{-1}
150	5.4 ± 2.0	1.7 ± 0.6
175	3.2 ± 1.2	2.6 ± 1.0
200	1.8 ± 0.7	4.4 ± 1.7
225	0.75 ± 0.24	9.9 ± 3.2
250	0.73 ± 0.14	10 ± 2
275	1.2 ± 0.4	5.9 ± 2.1

^{a} The uncertainty in $k_f^{(3)}$ and k_d results from the fitting procedure as well as the uncertainty in the partial He and SO_2 pressure.

The temperature dependent termolecular rate constants $k_f^{(3)}$ and the unimolecular decomposition rate constants k_d are summarized in Table 1. From this table it is apparent that $k_f^{(3)}$ decreases and k_d increases with increasing temperature. These temperature dependences are typical for ion–molecule reactions,[33,50] and can be explained in terms of the above-described energy transfer model for association reactions (cf. Section B.2) The unimolecular decomposition involves an activation barrier associated with the activation and cleavage of the $V_4O_{10}^-$–SO_2 bond, yielding a negative and positive temperature dependence for $k_f^{(3)}$ and k_d, respectively. Usually, this indicates a barrier-free interaction of $V_4O_{10}^-$ with SO_2.

The recorded $[V_4O_{10}, SO_2]^-$ signal does not represent the simple encounter complex **C** but instead a pyramidal structure (isomer **A**) is formed even at temperatures as low as 125 K (cf. Section C.1), which involves two activation barriers (cf. Fig. 2). The energy gained upon formation of the encounter complex **C**, which represents the first reaction step, is larger than the energy barriers associated with the transition states **TS1** and **TS3** (cf. Fig. 2). Consequently, there is always enough energy in the cluster complex available to overcome these activation barriers independent of the reaction temperature and the rate of stabilization k_s (cf. eqn (2b)). Thus, the barriers are not reflected in the experimental kinetic data. The experimental kinetics appear similar to those resulting in
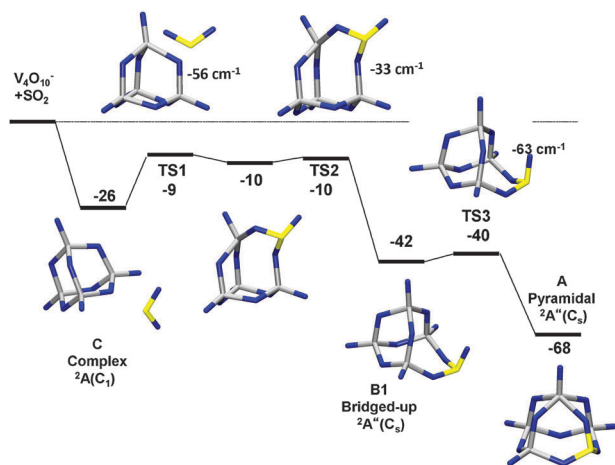

Fig. 2 DFT reaction energy profile for the formation of **A** for $[V_4O_{10}, SO_2]^-$ from $V_4O_{10}^-$ and SO_2. Relative energies are given in kJ mol^{-1}. For transition structures, the imaginary mode frequencies are also given.
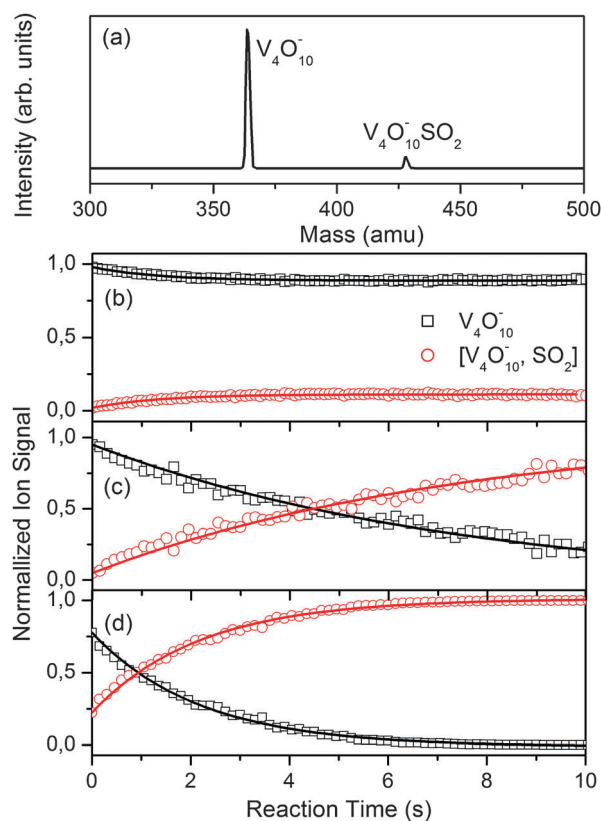

Fig. 3 (a) Mass spectrum of $V_4O_{10}^-$ after reaction with $(4.4 \pm 1.1) \times 10^{-3}$ Pa SO_2 for $t_R = 400$ ms at $T_R = 225$ K. (b)–(d) Selected kinetic data of the reaction of $V_4O_{10}^-$ with SO_2 at (b) $T_R = 275$ K and $p(SO_2) = (2.3 \pm 0.3) \times 10^{-3}$ Pa, (c) $T_R = 225$ K and $p(SO_2) = (4.4 \pm 1.1) \times 10^{-3}$ Pa, and (d) $T_R = 150$ K and $p(SO_2) = (6 \pm 2) \times 10^{-4}$ Pa. Open symbols represent the normalized intensities; solid lines are obtained by fitting with the integrated rate equations corresponding to eqn (4). Rate constants are given in Table 1.

the barrier-free formation of an encounter complex and the inverse reaction, i.e. the decomposition of isomer **A**, can be described by statistical unimolecular decay theories such as RRKM.

The determination of cluster–molecule binding energies employing RRKM theory has been described in detail before[31,50] and is only briefly outlined here. For the energized complex we used the computed frequencies of the $[V_4O_{10}, SO_2]^-$ ground state structure (**iso-A**), while the 'loose' TS model is employed. The 'loose' TS is suitable to model simple bond cleavage reactions but was also shown to be a most realistic model for more complex processes, such as those occurring in the dissociation of bare metal clusters.[51] For this TS model eight vibrations with large SO_2 contribution were selected and scaled by a factor $f = 0.5$ in addition to the removal of one mode ($V_4O_{10}^-$–SO_2 breathing mode with large amplitude on the S atom).[31,50–52] Furthermore, adiabatic rotations were taken into account by considering a temperature dependent rotational barrier, E_{RB}.[31,40] The resulting $V_4O_{10}^-$–SO_2 binding energy amounts to $E_0 = 0.72 \pm 0.12$ eV. Despite the very simplified model for $[V_4O_{10}, SO_2]^-*$ and the transition state and the rather complex theoretically predicted reaction pathway, the experimentally obtained binding energy is in

14348 | *Phys. Chem. Chem. Phys.*, 2012, **14**, 14344–14353

This journal is © the Owner Societies 2012

excellent agreement with the computed binding energy of 0.70 eV for **A**. This demonstrates that not the exact frequencies of the energized complex and the transition state but the frequency distribution and in particular the temperature dependence of the decomposition rate constants determine the binding energy.[31] To further demonstrate the insensitivity of the RRKM analysis on exact vibrational frequencies a second set of frequencies was employed. In this set the computed frequencies of the bare $V_4O_{10}^-$ cluster was used and the remaining frequencies were set equal to those of the free SO_2 molecule,[49] a cluster $-SO_2$ stretching frequency of 880 cm^{-1},[53,54] and five low frequency bending modes of 50 cm^{-1}.[31] This second set of vibrational frequencies resulted in $E_0 = 0.69 \pm 0.08$ eV, which falls well within the experimental uncertainty.

D SO$_2$ adsorption on $V_6O_{15}^-$, $V_8O_{20}^-$, $V_3TiO_{10}^-$, and $V_2Ti_2O_{10}^-$

Clusters size and cluster composition affect the characteristics of the SO_2 adsorption. The size dependency is investigated by considering the reaction kinetics of the $V_4O_{10}^-$, $V_6O_{15}^-$, $V_8O_{20}^-$ series. The influence of the electron configuration is studied by isomorphous substitution[25] of vanadium by titanium along the $V_4O_{10}^-$, $V_3TiO_{10}^-$, $V_2Ti_2O_{10}^-$ series. Before discussing the experimental reaction kinetic data, the energy profile of the reaction of $V_6O_{15}^-$ with SO_2 is calculated by DFT. It is shown that in this case the final product can only be formed after passing a transition structure with an energy well above the ground state energy of the educts.

D.1 DFT calculations of the energy profile for the reaction of $V_6O_{15}^-$ with SO_2

Using the same approach as for V_4O_{10} (see Section C.2), the structures of different $[V_6O_{15}, SO_2]^-$ isomers have been calculated by DFT. Moreover, the reaction energy profile for the formation of $[V_6O_{15}, SO_2]^-$ from $V_6O_{15}^-$ and SO_2 has been calculated (Fig. 4). Upon collision of $V_6O_{15}^-$ with SO_2 a $V_6O_{15}^- \cdot SO_2$ encounter complex, **C**, is formed. This encounter complex can only transform into a structure with SO_2 incorporated into the vanadium oxide framework after passing a transition structure for the reorganization, **TS1**, which is predicted at $+0.55$ eV above the educts. Once this transition structure is formed, the structure of the $[V_6O_{15}, SO_2]^-$ system sequentially goes through isomer **B'**, **TS2**, isomer **B**, and **TS3** (0.26 eV, 0.21 eV, 0.26 eV, and 0.26 eV, respectively, below the educts) to reach the most stable pyramidal isomer found in the present study, **A**. In **A** the SO_2 binding energy to $V_6O_{15}^-$ is 0.58 eV.

The structures of isomers **A** and **B** correspond to the pyramidal and bridging isomers of $V_7O_{18}^-$.[22]

The reaction energy profile of the reaction of $V_6O_{15}^-$ with SO_2 is characterized by the transition state **TS1** with an energy above that of the entrance channel. This implies that an activation step is needed to reach the transition state. According to the Lindemann energy transfer model for association reactions, the collision of $V_6O_{15}^-$ with SO_2 first yields the energized complex $[V_6O_{15}, SO_2]^{-*}$ (*cf.* eqn (2a)). The potential energy gain upon formation of the encounter complex **C**
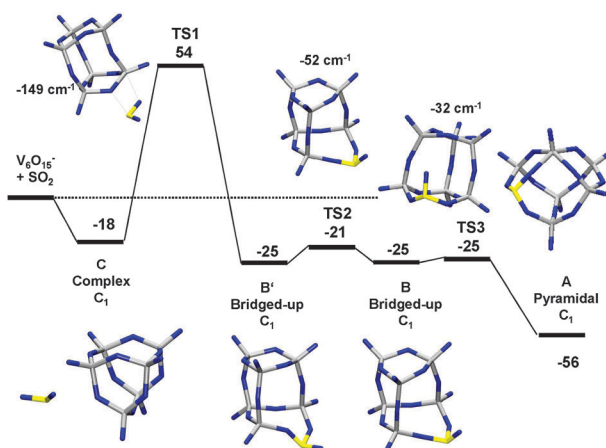

Fig. 4 DFT reaction energy profile for the formation of isomer **A** of $[V_6O_{15}, SO_2]^-$ from $V_6O_{15}^-$ and SO_2. Relative energies are given in kJ mol^{-1}. For transition structures, the imaginary mode frequencies are also given.

amounts to 0.17 eV, equivalent to the SO_2 binding energy. However, the experiments are performed in a temperature range of 250–175 K, which means that the encounter complex contains additional energy, namely, vibrational energy of the reactants before reaction and energy contained in the translational and rotational degrees of freedom that is converted into internal energy upon reaction. Following a rough estimate as proposed by Cox *et al.*[55] the total energy E^* contained in the energized complex $[V_6O_{15}, SO_2]^{-*}$ amounts to 1.08–1.47 eV in the investigated temperature range. Thus, the energy barrier associated with **TS1** of 0.75 eV can be easily overcome and the minimum energy structure **A** is likely to be formed. Even in the case of a fast stabilization of $[V_6O_{15}, SO_2]^{-*}$ by a He collision (*cf.* eqn (2b)) the internal energy of the thermal complex $[V_6O_{15}, SO_2]^-$ is sufficient to cross the energy barrier.

As outlined in Section B.2 and eqn (2a), the energized complex $[V_6O_{15}, SO_2]^{-*}$ can decompose unimolecularly back to the reactants with a rate constant k_d. As demonstrated in Section C.3 for $V_4O_{10}^-$, this rate constant can be used to determine experimental SO_2 binding energies by applying RRKM theory. However, in the case of $[V_6O_{15}, SO_2]^{-*}$ the decomposition rate constant is not determined by the activation barrier associated with the activation and cleavage of the $V_6O_{15}^- - SO_2$ bond, but instead by the considerably higher activation barrier associated with **TS1**. Due to this activation barrier the experimentally obtained k_d values decrease and an RRKM estimate of the binding energy would result in a too high value. Consequently, statistical RRKM theory cannot be applied to $V_6O_{15}^-$ to determine experimental binding energies due to the activation barrier that is higher than the energy of the educts.

D.2 Reaction kinetics of $V_6O_{15}^-$, $V_8O_{20}^-$, $V_3TiO_{10}^-$, and $V_2Ti_2O_{10}^-$

Fig. 5 displays selected ion mass distributions detected after storing $V_6O_{15}^-$, $V_8O_{20}^-$, $V_3TiO_{10}^-$, and $V_2Ti_2O_{10}^-$ in the ion trap in the presence of SO_2. The gas-phase reactions of the clusters with SO_2 are investigated at different ion trap
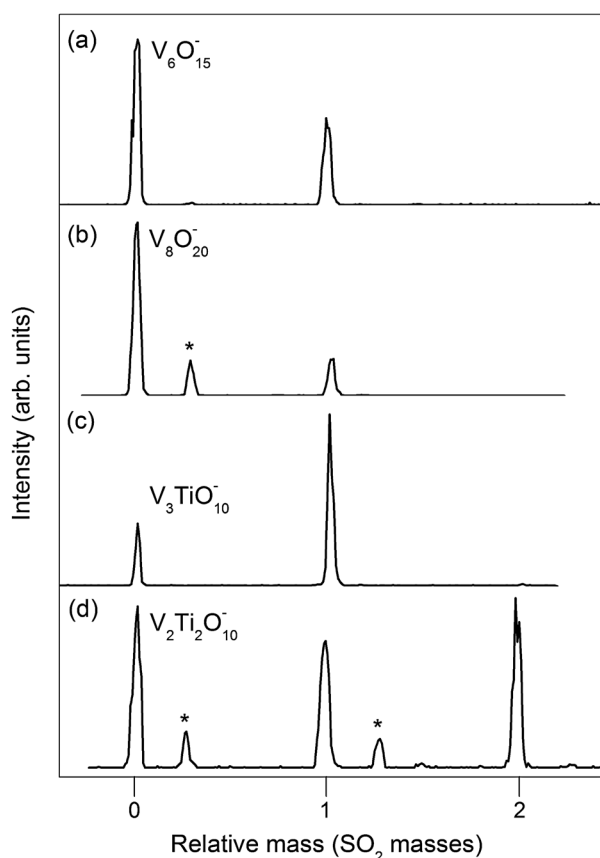
Fig. 5 Selected mass spectra obtained after reacting (a) $V_6O_{15}^-$, (b) $V_8O_{20}^-$, (c) $V_3TiO_{10}^-$, and (d) $V_2Ti_2O_{10}^-$ with SO_2. (a) $T_R = 200$ K, $p(SO_2) = (2.0 \pm 0.8) \times 10^{-4}$ Pa, $t_R = 400$ ms; (b) $T_R = 200$ K, $p(SO_2) = (4.0 \pm 1.0) \times 10^{-3}$ Pa, $t_R = 600$ ms; (c) $T_R = 225$ K, $p(SO_2) = (4.0 \pm 1.3) \times 10^{-4}$ Pa, $t_R = 600$ ms; (d) $T_R = 225$ K, $p(SO_2) = (4.0 \pm 1.6) \times 10^{-5}$ Pa, $t_R = 800$ ms. Mass peaks denoted with an asterisk correspond to complexes containing H_2O.

Fig. 6 Kinetic data of the reaction of (a) $V_6O_{15}^-$, (b) $V_8O_{20}^-$, (c) $V_3TiO_{10}^-$, and (d) $V_2Ti_2O_{10}^-$ with SO_2 at $T_R = 200$ K. Open symbols represent the normalized intensities. The solid lines are obtained by fitting with the corresponding integrated rate equations as discussed in the text. The dashed lines in (b) are obtained by assuming a competing reaction according to eqn (5a) and (5b) while the solid lines correspond to a displacement reaction given in eqn (5a) and (6). Rate constants are given in Table 2.

temperatures in the range of $T_R = 150$–275 K. In order to observe distinct reaction products within the time scale of the experiment, the applied partial SO_2 pressures are in the 3×10^{-4}–5×10^{-3} Pa ($V_4O_{10}^-$ and $V_8O_{20}^-$), 3×10^{-5}–3×10^{-4} Pa ($V_3TiO_{10}^-$ and $V_6O_{15}^-$), and 2×10^{-5}–5×10^{-5} Pa ($V_2Ti_2O_{10}^-$) ranges. Fig. 6 shows representative normalized product ion concentrations (open symbols) as a function of reaction time for $T_R = 200$ K and the solid lines represent fits of integrated rate equations of the proposed reaction mechanisms that are discussed below.

Similar to $V_4O_{10}^-$, the metal oxide clusters $V_6O_{15}^-$ and $V_3TiO_{10}^-$ adsorb, at all investigated ion trap temperatures, only one SO_2 molecule forming the complexes $[V_6O_{15}, SO_2]^-$ and $[V_3TiO_{10}, SO_2]^-$, respectively. The kinetics of these reactions are also best described by an equilibrium reaction mechanism at $T_R \geq 250$ K, while the backward reaction becomes negligible at $T_R < 250$ K. The termolecular rate constants $k_f^{(3)}$ exhibit a clearly negative temperature dependence (cf. Table 2), typically indicating energy barrier free adsorption of SO_2. This finding does not contradict the modelled reaction profile for $[V_6O_{15}, SO_2]^-$, predicting a considerable energy barrier for formation of the minimum energy structure.
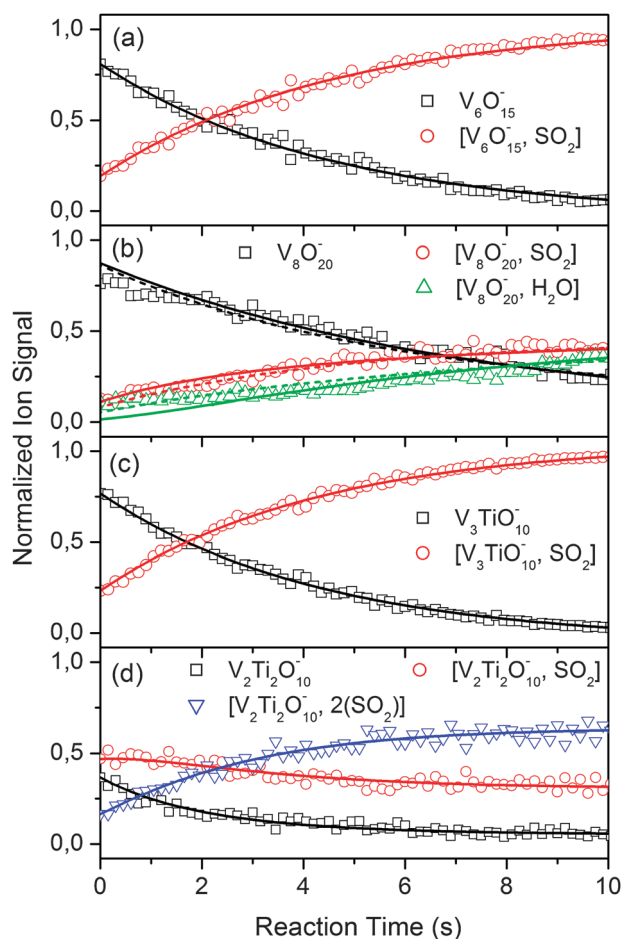
As discussed above, the energy E^* contained in the energized $[V_6O_{10}, SO_2]^{-*}$ complex is considerably larger than the energy barrier for all investigated temperatures and thus should be easily surmounted and cannot be seen in the temperature dependent experimental kinetic data. In fact, the strictly negative temperature dependence in the whole investigated temperature range indicates that the energy barrier can even be overcome at the lowest investigated reaction temperature of $T_R = 175$ K. The reaction does not stop at **C** as this should cause a considerable increase in k_d at low temperatures according to an RRKM estimate of the decomposition rate constants.

For $V_8O_{20}^-$ not only the SO_2 complex $[V_8O_{20}, SO_2]^-$, but also a water containing complex $[V_8O_{20}, H_2O]^-$ was recorded (cf. Fig. 5(b) and 6(b)). The H_2O presence indicates contamination of the inlet tubes and the ion trap, which are non-bakeable. $[V_8O_{20}, H_2O]^-$ has a high abundance relative to the amount of SO_2 complexes. Therefore, the reaction with H_2O must be taken into account in the reaction kinetics.

14350 | *Phys. Chem. Chem. Phys.*, 2012, **14**, 14344–14353
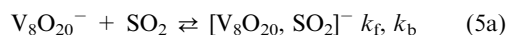
This journal is © the Owner Societies 2012

Table 2 Measured termolecular $k_f^{(3)}$ rate constants for the forward reaction between the metal oxide clusters and SO_2 and corresponding unimolecular decomposition rate constant k_d of the energized complex as a function of the reaction temperature T_R

	T_R/K	$k_f^{(3)}$/10^{-28} cm^6 s^{-1}	k_d/10^9 s^{-1}
$V_6O_{15}^-$	175	520 ± 240	0.015 ± 0.007
	200	120 ± 50	0.064 ± 0.029
	225	70 ± 30	0.11 ± 0.06
	250	43 ± 25	0.16 ± 0.10
$V_8O_{20}^-$	150	12 ± 5^a	0.68 ± 0.30
		3.5 ± 1.6^b	2.4 ± 1.1
	175	6.7 ± 2.5^a	1.2 ± 0.4
		1.7 ± 0.6^b	4.7 ± 1.8
	200	0.47 ± 0.21^a	16 ± 7
		0.29 ± 0.12^b	26 ± 11
	225	0.078 ± 0.030	91 ± 34
$V_3TiO_{10}^-$	150	200 ± 100	0.045 ± 0.024
	175	160 ± 70	0.051 ± 0.023
	200	80 ± 30	0.10 ± 0.03
	225	60 ± 19	0.13 ± 0.05
	250	38 ± 16	0.22 ± 0.08
	275	13 ± 6	0.53 ± 0.25
$V_2Ti_2O_{10}^-$	200	500 ± 250	0.016 ± 0.008
	225	660 ± 340	0.011 ± 0.006
	250	130 ± 70	0.055 ± 0.028

[a] Assuming a H_2O/SO_2 displacement reaction (eqn (5a) and (5b)).
[b] Assuming a H_2O/SO_2 competing reaction (eqn (5a) and (6)).

The formation of $[V_8O_{20}, SO_2]^-$ and $[V_8O_{20}, H_2O]^-$ might result from competitive SO_2 and H_2O adsorption on $V_8O_{20}^-$:

$$V_8O_{20}^- + SO_2 \rightleftarrows [V_8O_{20}, SO_2]^-\ k_f, k_b \quad (5a)$$

$$V_8O_{20}^- + H_2O \rightleftarrows [V_8O_{20}, H_2O]^- \quad (5b)$$

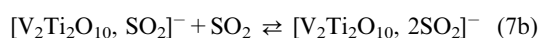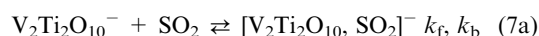An alternative possible reaction mechanism is first formation of the $[V_8O_{20}, SO_2]^-$ complex, according to eqn (5a), and the subsequent displacement of SO_2 by H_2O:

$$[V_8O_{20}, SO_2]^- + H_2O \leftrightarrows [V_8O_{20}, H_2O]^- + SO_2 \quad (6)$$

The lines in Fig. 6(b) represent the fits of the competing (dashed lines) and displacement (solid lines) reaction mechanism to the experimental kinetic data, both exhibiting comparable fit quality. Thus, none of the proposed reaction mechanisms can be unambiguously assigned and in Table 2 the termolecular rate constants obtained by fitting both mechanisms are listed. Since H_2O is only present in the ion trap as a residual gas and thus of unknown concentration, the reaction steps (5b) and (6) are not further discussed. At the highest investigated reaction temperature, $T_R = 225$ K, the intensity of the H_2O complexes was very small and eqn (5a) was used to fit the data.

In contrast to $V_4O_{10}^-$, $V_6O_{15}^-$, $V_8O_{20}^-$, and $V_3TiO_{10}^-$, which only adsorb one SO_2 molecule, the bimetallic oxide cluster $V_2Ti_2O_{10}^-$ is more reactive. From Fig. 6(d) it is apparent that the first formed product $[V_2Ti_2O_{10}, SO_2]^-$ further reacts under the addition of a second SO_2 ligand, yielding $[V_2Ti_2O_{10}, 2SO_2]^-$. The reaction mechanism that best fits the kinetic data is given by:

$$V_2Ti_2O_{10}^- + SO_2 \rightleftarrows [V_2Ti_2O_{10}, SO_2]^-\ k_f, k_b \quad (7a)$$

$$[V_2Ti_2O_{10}, SO_2]^- + SO_2 \rightleftarrows [V_2Ti_2O_{10}, 2SO_2]^- \quad (7b)$$

and the fits are shown as solid lines in Fig. 6(d). Besides $[V_2Ti_2O_{10}, SO_2]^-$ and $[V_2Ti_2O_{10}, 2SO_2]^-$ two additional low intensity products are detected, corresponding to the water complexes $[V_2Ti_2O_{10}, H_2O]^-$ and $[V_2Ti_2O_{10}, SO_2, H_2O]^-$ (cf. Fig. 5(d)). However, since these $[V_2Ti_2O_{10}, H_2O]^-$ complexes are only detected at the lowest investigated reaction temperatures and are present in significantly smaller amounts than the SO_2 complexes, they can be neglected in the fitting procedure. Eqn (7a) and (7b) describe the reaction of $V_2Ti_2O_{10}^-$ with SO_2 satisfactorily.

Similar to $V_4O_{10}^-$ and $V_6O_{15}^-$, also $V_8O_{20}^-$ and the Ti doped clusters $V_3TiO_{10}^-$ and $V_2Ti_2O_{10}^-$ exhibit a negative temperature dependence of $k_f^{(3)}$, indicating either a barrier-free adsorption of SO_2 or activation barriers that can be easily surmounted in the whole investigated temperature range.

D.3 Size and composition dependence

For none of the clusters investigated here, evidence for the formation of SO_3 was found. This is in line with the calculations by Jakubikova and Bernstein, who demonstrated that only oxygen-rich vanadium oxide clusters convert SO_2 into SO_3.[15] The reaction constants for the SO_2 association and desorption reactions appear to depend strongly on the cluster size and composition. The rate constants increase upon titanium for vanadium substitution and are higher for $V_6O_{15}^-$ than for $V_4O_{10}^-$ or $V_8O_{20}^-$. Since the size and composition dependence of k_a and k_s are marginal, an increase in the termolecular rate constant is according to eqn (3) caused by a decreased unimolecular rate constant k_d or an increased life time of the energized complex $[V_mTi_nO_o, SO_2]^-*$. Three factors (or a combination of them) can cause this increased life time: (i) a higher SO_2 binding energy to the cluster, (ii) a higher activation barrier for formation of a stable complex which hampers the unimolecular dissociation, and (iii) a higher number of degrees of freedom among which the energy gained upon complex formation can be redistributed. The last factor is only relevant when comparing reaction rates of clusters with different size.

Based on these three factors the cluster size dependent reactivity toward SO_2 can be understood. The unimolecular decomposition of $[V_6O_{15}, SO_2]^-*$ is found to be slower than that of $[V_4O_{10}, SO_2]^-*$. Factor (i) does not explain this observation since the SO_2 binding energy to $V_6O_{15}^-$ is 0.58 eV, which is lower than the corresponding value for $V_4O_{10}^-$ (0.70 eV). It is the activation barrier (**TS1** at $+ 0.58$ eV) for formation of the minimum energy structure **A** of $[V_6O_{15}, SO_2]^-*$ which reduces the unimolecular dissociation rate constant k_d, i.e. factor (ii). In addition, the increased number of vibrational degrees of freedom in the larger $[V_6O_{15}, SO_2]^-*$ complex compared to $[V_4O_{10}, SO_2]^-*$ further increases the life time of the energized complex. The largest investigated vanadium oxide cluster $[V_8O_{20}, SO_2]^-*$ exhibits unimolecular decomposition rate constants k_d, which are up to one order of magnitude larger (depending on the reaction temperature and the proposed reaction mechanism) than those of $[V_4O_{10}, SO_2]^-*$. The high unimolecular decomposition rate of $[V_8O_{20}, SO_2]^-*$ cannot be explained by factors (ii) and (iii). The larger complex $[V_8O_{20}, SO_2]^-*$ comprises nearly twice as many vibrational

degrees of freedom as $[V_4O_{10}, SO_2]^-*$. In addition, the energy profile of the reaction of $V_4O_{10}^-$ with SO_2 reveals only marginal energy barriers for formation of isomer **A** (see Fig. 2). Consequently, the reactivity of $V_8O_{20}^-$ can only be explained by a lower binding energy of the SO_2 molecule.

$V_4O_{10}^-$, $V_3TiO_{10}^-$, and $V_2Ti_2O_{10}^-$ all contain the same number of atoms and thus the same number of vibrational degrees of freedom to accommodate the energy gained upon reaction with SO_2. However, they exhibit very different reactivity with unimolecular decomposition rate constants differing by up to three orders of magnitude depending on T_R. Independent of the composition, the clusters have a tetrahedral shape.[25] However, electronically they are very different. While $V_4O_{10}^-$ has a single unpaired electron, $V_3TiO_{10}^-$ is a closed shell species isoelectronic with the neutral V_4O_{10}. It has fully oxidized vanadium and titanium atoms, in which the V, Ti and O atoms carry a formal valence of $+v$, $+iv$, and $-ii$, respectively. Although $V_3TiO_{10}^-$ is a closed shell species, it surprisingly is more reactive than $V_4O_{10}^-$. The reason for the higher reactivity of $V_3TiO_{10}^-$ likely is the charge localization on the outer oxygen atom that binds with the titanium and acts as the active site for the SO_2 adsorption. $V_2Ti_2O_{10}^-$ has a doublet ground state with a free radical localized on a singly titanium-bonded terminal oxygen atom.[25] This radical is likely transferred to the first SO_2 molecule. The second SO_2 molecule can then bind to a similar site as in $V_3TiO_{10}^-$. The presence of the oxygen radical explains the much higher reactivity of $V_2Ti_2O_{10}^-$ and the observation that it likes to bind two SO_2 molecules.

E. Conclusions

Using gas phase IRMPD spectroscopy in conjunction with DFT calculations we have shown that upon adsorption the SO_2 molecule is incorporated in the vanadium-oxide framework of $V_4O_{10}^-$. The $[V_4O_{10}, SO_2]^-$ complex has a square pyramidal structure similar to $V_5O_{13}^-$ where one of the $O{=}VO_{3/2}$ corners of the square has been replaced by $S^{(+)}O_{3/2}$, and the $O{=}V(d^0)^{(-)}O_{4/2}$ top site has been replaced by a $O{=}V(d^1)^{(2-)}O_{4/2}$ site with the unpaired electron localized in d-states of this vanadium atom. The calculated SO_2 binding energy of 0.70 eV agrees nicely with the experimental value of $E_0 = 0.72 \pm 0.12$ eV, which was determined from the kinetic data using the Lindemann energy transfer model for association reactions in conjunction with statistical RRKM theory.

The reaction energy profiles of $V_4O_{10}^- + SO_2$ and $V_6O_{15}^- + SO_2$ have been modelled. Whereas the transition states in the reaction of $V_4O_{10}^-$ with SO_2 have energies below that of the separated partners, the reaction of $V_6O_{15}^-$ with SO_2 proceeds *via* a transition state with energy higher than the ground state energy of the educts.

The role of cluster size and composition is investigated by studying the reaction kinetics of larger ($V_6O_{15}^-$ and $V_8O_{20}^-$) and titanium doped ($V_3TiO_{10}^-$ and $V_2Ti_2O_{10}^-$) vanadium oxide clusters with SO_2. The cluster size dependence is discussed in terms of three factors: (1) the SO_2 binding energy, (2) activation barriers involved in the formation of the minimum energy structure, and (3) the number of vibrational degrees of freedom which are available to accommodate the energy gained upon reaction.

The higher reactivity of the titanium doped clusters is attributed to the charge localization on the outer oxygen atom that binds with the titanium atom in $V_3TiO_{10}^-$. The presence of a free radical localized on a singly titanium-bonded terminal oxygen atom in $V_2Ti_2O_{10}^-$ allows binding of a second SO_2 molecule.

The results of the present gas phase study provide new ideas about the reaction mechanism of vanadium oxide nanoparticles with SO_2, which are of relevance for a deeper understanding and eventually further optimization of specific catalytic cycles such as the SO_3 production from SO_2 using vanadium oxide particles.

References

1 G. Ertl, H. Knotzinger and J. Weitkamp, *Handbook of Heterogeneous Catalysis*, Wiley-VCH, Weinheim, 1997.
2 J. P. Dunn, H. G. Stenger and I. E. Wachs, *Catal. Today*, 1999, **51**, 301.
3 P. J. Chenier, *Survey of Industrial Chemistry*, Kluwer, New York, 3rd edn, 2002.
4 O. B. Lapina, B. S. Bal'zhinimaev, S. Boghosian, K. M. Eriksen and R. Fehrmann, *Catal. Today*, 1999, **51**, 469.
5 A. J. Leavitt, R. B. Wyrwas, W. T. Wallace, D. S. Serrano, M. G. Arredondo, L. M. Leslie, F. A. Khan and R. L. Whetten, *J. Phys. Chem. A*, 2005, **109**, 6218.
6 R. C. Bell, K. A. Zemski, D. R. Justes and A. W. Castleman, Jr., *J. Chem. Phys.*, 2001, **114**, 798.
7 K. A. Zemski, D. R. Justes and A. W. Castleman, Jr., *J. Phys. Chem. A*, 2001, **105**, 10237.
8 S. Feyel, J. Döbler, D. Schröder, J. Sauer and H. Schwarz, *Angew. Chem., Int. Ed.*, 2006, **45**, 4681.
9 S. Feyel, D. Schröder and H. Schwarz, *J. Phys. Chem. A*, 2006, **110**, 2647.
10 S. Li, A. Mirabal, J. Demuth, L. Wöste and T. Siebert, *J. Am. Chem. Soc.*, 2008, **130**, 16832.
11 Y. X. Zhao, X. N. Wu, J. B. Ma, S. G. He and X. L. Ding, *J. Phys. Chem. C*, 2010, **114**, 12271.
12 A. Fielicke, R. Mitrić, G. Meijer, V. Bonačić-Koutecký and G. Von Helden, *J. Am. Chem. Soc.*, 2003, **125**, 15716.
13 T. Wende, J. Döbler, L. Jiang, P. Claes, E. Janssens, P. Lievens, G. Meijer, K. R. Asmis and J. Sauer, *Int. J. Mass Spectrom.*, 2010, **297**, 102.
14 R. B. Wyrwas, *Vanadium Oxide Anion Clusters: Their Abundances, Structures, and Reactions with SO₂*, Georgia Institute of Technology, 2004.
15 E. Jakubikova and E. R. Bernstein, *J. Phys. Chem. A*, 2007, **111**, 13339.
16 S. G. He, Y. Xie, F. Dong, S. Heinbuch, E. Jakubikova, J. J. Rocca and E. R. Bernstein, *J. Phys. Chem. A*, 2007, **111**, 13339.
17 A. Fielicke and K. Rademann, *Phys. Chem. Chem. Phys.*, 2002, **4**, 2621.
18 K. R. Asmis, G. Santambrogio, M. Brümmer and J. Sauer, *Angew. Chem., Int. Ed.*, 2005, **44**, 3122.

19 K. R. Asmis, M. Brümmer, C. Kaposta, G. Santambrogio, G. von Helden, G. Meijer, K. Rademann and L. Wöste, *Phys. Chem. Chem. Phys.*, 2002, **4**, 1101.

20 M. Brümmer, C. Kaposta, G. Santambrogio and K. R. Asmis, *J. Chem. Phys.*, 2003, **119**, 12700.

21 K. R. Asmis, G. Meijer, M. Brümmer, C. Kaposta, G. Santambrogio, L. Wöste and J. Sauer, *J. Chem. Phys.*, 2004, **120**, 6461.

22 G. Santambrogio, M. Brümmer, L. Wöste, J. Döbler, M. Sierka, J. Sauer, G. Meijer and K. R. Asmis, *Phys. Chem. Chem. Phys.*, 2008, **10**, 3992.

23 S. F. Vyboishchikov and J. Sauer, *J. Phys. Chem. A*, 2001, **105**, 8588.

24 K. R. Asmis, T. Wende, M. Brümmer, O. Gause, G. Santambrogio, E. C. Stanca-Kaposta, J. Döbler, A. Niedziela and J. Sauer, *Phys. Chem. Chem. Phys.*, 2012, **14**, 9377.

25 E. Janssens, G. Santambrogio, M. Brümmer, L. Wöste, P. Lievens, J. Sauer, G. Meijer and K. R. Asmis, *Phys. Rev. Lett.*, 2006, **96**, 233401.

26 H. J. Zhai and L. S. Wang, *J. Chem. Phys.*, 2002, **117**, 7882.

27 K. R. Asmis, M. Brümmer, C. Kaposta, G. Santambrogio, G. v. Helden, G. Meijer, K. Rademann and L. Wöste, *Phys. Chem. Chem. Phys.*, 2002, **4**, 1101.

28 E. Janssens, H. Tanaka, S. Neukermans, R. E. Silverans and P. Lievens, *Phys. Rev. B: Condens. Matter Mater. Phys.*, 2004, **69**, 085402.

29 T. M. Bernhardt, *Int. J. Mass Spectrom.*, 2005, **243**, 1.

30 D. Oepts, A. F. G. van der Meer and P. W. van Amersfoort, *Infrared Phys. Technol.*, 1995, **36**, 297.

31 T. M. Bernhardt, J. Hagen, S. M. Lang, D. M. Popolan, L. D. Socaciu-Siebert and L. Wöste, *J. Phys. Chem. A*, 2009, **113**, 2724.

32 E. Schuhmacher, *DETMECH – Chemical Reaction Kinetics Software*, University of Bern, 2003 (http://www.chemsoft.ch).

33 J. I. Steinfeld, J. S. Francisco and W. L. Hase, *Chemical Kinetics and Dynamics*, Prentice Hall, Upper Saddle River, 2nd ed., 1999.

34 P. Langevin, *Ann. Chim. Phys.*, 1905, **5**, 245.

35 *Handbook of Chemistry and Physics*, ed. D. R. Lide, CRC, Boca Raton, 1995.

36 D. Patel, D. Margolese and T. R. Dyke, *J. Chem. Phys.*, 1979, **70**, 2740.

37 T. Su, *J. Chem. Phys.*, 1988, **89**, 5354.

38 R. A. Marcus, *J. Chem. Phys.*, 1952, **20**, 359.

39 K. A. Holbrook, M. J. Pillings and S. H. Robertson, *Unimolecular Reactions*, Wiley, Chichester, 2nd ed., 1996.

40 L. Drahos and K. Vékey, *J. Mass Spectrom.*, 2001, **36**, 237.

41 R. Ahlrichs, M. Bär, M. Häser, H. Horn and C. Kölmel, *Chem. Phys. Lett.*, 1989, **162**, 165.

42 A. D. Becke, *Phys. Rev. A*, 1988, **38**, 3098.

43 A. Schäfer, C. Huber and R. Ahlrichs, *J. Chem. Phys.*, 1994, **100**, 5829.

44 A. J. Wachters, *J. Chem. Phys.*, 1970, **52**, 1033.

45 C. W. Bauschlicher, Jr. and H. Partridge, *Chem. Phys. Lett.*, 1995, **240**, 533.

46 T. H. Dunning, Jr., K. A. Peterson and A. K. Wilson, *J. Chem. Phys.*, 2001, **114**, 9244.

47 P. Deglmann, F. Furche and R. Ahlrichs, *Chem. Phys. Lett.*, 2002, **362**, 511.

48 K. R. Asmis and J. Sauer, *Mass Spectrom. Rev.*, 2007, **26**, 542.

49 W. B. Person and G. Zerbi, *Vibrational Intensities in Infrared and Raman Spectroscopy*, Elsevier, Amsterdam, 1982.

50 S. M. Lang, T. M. Bernhardt, R. N. Barnett and U. Landman, *ChemPhysChem*, 2010, **11**, 1570.

51 V. A. Spasov, T. H. Lee, J. P. Maberry and K. M. Ervin, *J. Chem. Phys.*, 1999, **110**, 5208.

52 M. F. Jarrold and J. E. Bower, *J. Chem. Phys.*, 1987, **87**, 5728.

53 S. Boghosian, *J. Chem. Soc., Faraday Trans.*, 1998, **94**, 3463.

54 I. Giakoumelou, R. M. Caraba, V. I. Parvulescu and S. Boghosian, *Catal. Lett.*, 2002, **78**, 209.

55 D. M. Cox, K. C. Reichmann, D. J. Trevor and A. Kaldor, *J. Chem. Phys.*, 1988, **88**, 111.